STEM CELLS TRANSLATIONAL MEDICINE

TISSUE-SPECIFIC PROGENITOR AND STEM CELLS

HDAC8, A Potential Therapeutic Target, Regulates Proliferation and Differentiation of Bone Marrow Stromal Cells in Fibrous Dysplasia

TAO XIAO,[a,b,*] YU FU,[a,b,*] WEIWEN ZHU,[a] RONGYAO XU,[a] LING XU,[a] PING ZHANG,[a,b] YIFEI DU,[b] JIE CHENG,[a] HONGBING JIANG [a,b]

[a]Jiangsu Key Laboratory of Oral Diseases, Nanjing Medical University, Nanjing, People's Republic of China; [b]Department of Oral and Maxillofacial Surgery, Affiliated Hospital of Stomatology, Nanjing Medical University, Nanjing, People's Republic of China

*Contributed equally.

Correspondence: Hongbing Jiang, Ph.D., Jiangsu Key Laboratory of Oral Diseases, Nanjing Medical University, No.136, Hanzhong Road, Nanjing, Jiangsu Province 210029, People's Republic of China. Telephone: +86-25-85031914; e-mail: jhb@njmu.edu.cn

Received March 15, 2018; accepted for publication August 15, 2018; first published November 13, 2018.

http://dx.doi.org/10.1002/sctm.18-0057

Key Words. Fibrous dysplasia of bone • Histone deacetylase 8 • Histone deacetylase inhibitors • Mesenchymal stromal cells • Osteogenesis • Signal transduction

ABSTRACT

Fibrous dysplasia (FD) is a disease of postnatal skeletal stem cells caused by activating mutations of guanine nucleotide-binding protein alpha-stimulating activity polypeptide (*GNAS*). FD is characterized by high proliferation and osteogenesis disorder of bone marrow stromal cells (BMSCs), resulting in bone pain, deformities, and fractures. The cAMP-CREB pathway, which is activated by *GNAS* mutations, is known to be closely associated with the occurrence of FD. However, so far there is no available targeted therapeutic strategy for FD, as a critical issue that remains largely unknown is how this pathway is involved in FD. Our previous study revealed that histone deacetylase 8 (*HDAC8*) inhibited the osteogenic differentiation of BMSCs via epigenetic regulation. Here, compared with normal BMSCs, FD BMSCs exhibited significantly high proliferation and weak osteogenic capacity in response to *HDAC8* upregulation and tumor protein 53 (*TP53*) downregulation. Moreover, inhibition of cAMP reduced *HDAC8* expression, increased *TP53* expression and resulted in the improvement of FD phenotype. Importantly, *HDAC8* inhibition prevented cAMP-induced cell phenotype and promoted osteogenesis in nude mice that were implanted with FD BMSCs. Mechanistically, *HDAC8* was identified as a transcriptional target gene of CREB1 and its transcription was directly activated by CREB1 in FD BMSCs. In summary, our study reveals that *HDAC8* associates with FD phenotype and demonstrates the mechanisms regulated by cAMP-CREB1-HDAC8 pathway. These results provide insights into the molecular regulation of FD pathogenesis, and offer novel clues that small molecule inhibitors targeting *HDAC8* are promising clinical treatment for FD.
STEM CELLS TRANSLATIONAL MEDICINE *2019;8:148–161*

SIGNIFICANCE STATEMENT

Histone deacetylase 8 (*HDAC8*) is firstly identified as a novel gene tightly associated with enhanced proliferation and impaired osteogenic differentiation of bone marrow stromal cells (BMSCs) from fibrous dysplasia (FD). This research is focused on the role of the cAMP-CREB1-HDAC8 pathway in regulating biological characteristics of FD BMSCs. Moreover, *HDAC8* inhibition is evaluated to have significant therapeutic effects in experimental models of FD in vitro as well as in nude mice that are implanted with FD BMSCs. The results demonstrate an important link between *HDAC8* and the bone maturity of BMSCs and suggest that a specific HDAC8 inhibitor may be beneficial for FD therapy.

INTRODUCTION

Fibrous dysplasia (FD), a non-hereditary and benign bone disease, is characterized by the replacement of normal bone and marrow by a mixture of fibrous tissue and immature trabecular bone [1]. FD in the craniofacial area can result in serious orofacial deformities, bone pain, dental disorders, and pathologic fractures [2, 3]. Currently, the pathogenesis of FD remains unclear, and thus there is still no cure; treatment largely consists of osteoclastic suppressor related-drugs and surgical intervention to reconstruct lesion sites [4, 5]. According to recent studies, FD is considered to be a skeletal stem cell disease that evolves from somatic activating missense mutations in the guanine nucleotide-binding protein alpha-stimulating activity polypeptide (*GNAS*) gene of bone marrow stromal cells (BMSCs). The *GNAS* mutation results in the overproduction of

cAMP and subsequent abnormal molecular and cellular responses [6–8].

With the excessive production of cAMP, phosphorylation of cAMP-response element binding protein (CREB) is directly activated by cAMP-dependent protein kinase (PKA), which promotes the transcription of downstream genes through CREB binding to the cAMP-response element (CRE) in the promoter regions of related genes [9–11]. Recent studies have shown that osteogenesis-related transcription factors such as runt-related transcription factor 2 (*RUNX2*) and special protein 7 (*SP7*) are mediated individually and are closely associated with the activation of transcription in response to cAMP, which leads to impaired osteogenic differentiation in FD lesions [2, 12]. However, the detailed molecular and cellular mechanisms underlying the cAMP-CREB signaling pathway regulation of osteoblast-related transcription factors in FD remain largely unexplored.

Histone deacetylation (HDAC) is a key component in regulation of gene expression by mediating acetylation status of histones in promoters of genes. A plenty of evidence has indicated the negative regulation of HDACs in bone formation. HDAC1 downregulates the level of acetylation of histone in the promoters of osteoblast marker genes, including *SP7* and *BGLAP*, resulting in the inhibited osteogenesis of BMSCs [13]. The inhibitor of HDAC2 enhances osteoblast differentiation through upregulating the expression of SPP1 and bone sialoprotein [14]. HDAC3-7 lead to impaired osteogenic potential by repressing *Runx2* transcriptional activity in a deacetylation-dependent manner or binding with *RUNX2* protein in the HDACs interaction domain [15–19]. Among these, *HDAC8* specifically controls craniofacial skeletal patterning by repressing a subset of transcription factors and *HDAC8* has been shown to regulate these genes via epigenetic DNA modification [20]. Our previous study indicated that *HDAC8* functioned as a transcriptional repressor by regulating the level of acetylation of H3 at Lys9 (H3K9Ac) and by interacting with *RUNX2* during the osteogenesis of BMSCs [21]. Based on these reports, we proposed that *HDAC8* may be related to the suppressive osteogenic potential of BMSCs in FD.

In addition, an increased proliferative ability that leads to fibrotic lesions in FD is the other main feature of FD BMSCs, resulting from the overproduction of cAMP [22]. The inhibitory effects of increased cAMP on the expression of tumor protein 53 (*TP53*) and DNA damage-induced apoptosis are dependent on HDAC activity [23]. *HDAC8* knockdown results in the decreased proliferation via elevated *TP53* expression [24, 25]. However, few studies have reported regulatory role for *HDAC8* related to *TP53* expression in BMSCs and *TP53*-dependent apoptosis. Here, we investigated how cAMP and *HDAC8* regulate proliferation and apoptosis in FD BMSCs via *TP53*.

In present study, we aimed to explore the properties of FD BMSCs and to reveal that the high expression of *HDAC8* leads to increased proliferative ability, decreased apoptosis and impaired osteogenic differentiation potential of FD BMSCs due to its inhibition of *TP53* and *RUNX2*. We further unraveled the pivotal role of cAMP-CREB1 pathway in the development and progression of FD by promoting *HDAC8* transcription. Our study demonstrates that the cAMP-CREB1-HDAC8 pathway is critically involved in the pathologic mechanism underlying craniofacial FD. These results suggest that therapeutic intervention targeting the cAMP-CREB1-HDAC8 axis might be beneficial for offering novel clues to the clinical treatment of FD.

Materials and Methods

Patients and Samples

A total of 42 cases of craniofacial FD were retrieved from the Hospital of Stomatology affiliated with Nanjing Medical University, (Nanjing, Jiangsu, China) from 2005 to 2017. Formalin-fixed, paraffin-embedded tissues of the FD patients were obtained for mutational analysis. According to previous methods [26], all cases were re-evaluated and confirmed by experienced professionals according to the current clinical, radiographic, and histopathological guidelines for FD.

Mutation Analysis

Genomic DNA from paraffin-embedded tissues of the FD patients was extracted by a QIAamp DNA FFPE Tissue Kit (Qiagen, Duesseldorf, Hilden, Germany). An approximately 600 bp DNA sequence of *GNAS* (NCBI Gene ID 2778) was chosen as the target for allele-specific PCR amplification. The following PCR primer sequences were used: wild-type, 5-GACCTGCTTCGCTGG*CG-3; R201H, 5-GGACCTGCTTCG CTGG*C (A)-3; R201C, 5 -CAGGACCTGCTTCGCTC*C(T)-3 (where * denotes internal mismatching and parentheses denotes the base transition); and reverse, 5 -TCTTGCTTGTTGAGGAACAG-3. TaKaRa Taq Version 2.0 plus dye (TaKaRa, Shiga, Tokyo, Japan) was used for PCR amplification. Subsequently, the product was examined by agarose gel electrophoresis, and the sequencing was performed by General Biosystems (Chuzhou, Anhui, China).

Cell Culture

Under a protocol approved by the Ethics and Research Committee of Nanjing Medical University, fresh FD tissues were immediately obtained from bone lesions for primary cell culture after surgical removal. FD lesions of the jaw were obtained from three volunteer patients (patient 1, 31-year-old, male, maxilla, *GNAS* R201H; patient 2, 27-year-old, female, mandible, *GNAS* R201C; and patient 3, 12-year-old, male, maxilla and mandible, *GNAS* R201H). As a control, normal jaw was obtained from donors (20- to 25-year-old, a total of six cases of healthy donors) when they underwent impacted tooth extraction or dental implantation at our hospital. Informed consent was obtained before volunteers were enrolled in this study. Primary BMSCs were cultured in 25 cm^2 plastic flasks with medium consisting of DMEM (Gibco, Grand Island, NY, USA), 100 U/ml penicillin and 100 μg/ml streptomycin, and 10% fetal bovine serum (ScienCell, Carlsbad, CA, USA) at 37°C maintained in 5% CO_2. The medium was changed every 3 days until 80%–90% confluence was achieved. BMSCs from FD lesions and normal jaw were used in passages 3–5 throughout the experiments.

Detection of Apoptosis

A flow cytometry-based apoptosis assay was performed using propidium iodide (PI)/Annexin V-FITC or 7-amino-actinomycin D (7-AAD)/Annexin V-PE (Univ-bio, Shanghai, China). Approximately 1×10^6 cells were trypsinized and were resuspended in 500 μl of ×1 binding buffer. Subsequently, 5 μl of PI and 5 μl of Annexin V-FITC were added. (7-AAD and Annexin V-PE were added to FD BMSCs transfected with LeV-scramble/shHDAC8). The suspensions were incubated for 10 minutes at

room temperature, and counts were taken with a FACSverse (BD, San Jose, CA, USA). Quadrant analysis of the data was performed using FlowJo 7.6.1. The assays were performed in triplicate and the results were presented as quantitative histogram. The bromodeoxyuridine (BrdU) assay was performed as previously described [27].

cAMP Extraction and Measurement

For measurement of intracellular levels of cAMP, the cells plated in 12-well plates were incubated for 1 hour in serum-free medium containing 1 mM 3-isobutyl-1-methylxanthine (Sigma, St. Louis, MO, USA). Then, cAMP was extracted by 0.1 M HCl for 20 minutes and the lysate was immediately centrifuged at 1,000*g* for 10 minutes at 4°C. The supernatant was collected and used directly for measurement of cAMP level or stored at −80°C before measurement using a Cyclic AMP ELISA Kit (Cayman, Ann Arbor, MI, USA), according to the manufacturer's instructions. The assays were performed in in triplicate and the results were expressed as picomoles/milligram protein (pmoles/mg protein). The immunofluorescent staining assay was performed as we described previously [28].

Differentiation and Alizarin Red Staining

To achieve the osteogenic differentiation of FD BMSCs in vitro, cells were cultured in complete medium supplemented with 50 μM ascorbic acid (Sigma), 10 mM β-glycerophosphate (Sigma), and 10^{-7} M dexamethasone (Sigma). The medium was changed every 3 days. The mineralization potential of BMSCs was assessed via Alizarin Red staining when cells were cultured with osteogenic medium for 14 days. For Alizarin Red staining, the cells were fixed in anhydrous alcohol for 30 minutes, followed by rinsing with double-distilled H_2O. Subsequently, cells were stained with 2% Alizarin Red S (pH 4.2) (Sigma) for 10 minutes. The deposition of calcium was identified under light microscope. Calcified nodules were eluted with 10% cetylpyridinium chloride and the absorbance at 562 nm was compared to calcium standards.

Lentiviral Transfection and RNA Interference

FD BMSCs were transfected with lentiviral vectors expressing the scramble shRNA (LeV-scramble) or the *HDAC8* shRNA (LeV-shHDAC8) in the presence of polybrene (8 mg/ml). The shHDAC8 sequences were: shHDAC8-1: 5-GCAAGTGTCTTAAG TACATCC-3; shHDAC8-2: 5-GGATTTGGATCTGCACCATGG-3; shHDAC8-3: 5-GG TCCCGGTTTATATCTATAG-3 and scramble shHDAC8: 5-TTCTCCG AACGTGT CACGT-3. Small interfering RNA (siRNA) targeting CREB1 and scramble siRNA were purchased from GenePharma (Shanghai, China). The siRNA sequences were: siCREB1-1: 5-GCCACAGAUUGCCACAUUATT-3, 5-UAAUGUGGCA AUCUGUGGC TT-3; siCREB1-2: 5-GCCAACUCCAAUUUACCAATT-3, 5-UUG GU AAAUUGGAGUUGGCTT-3; siCREB1-3: 5-GCCUGCAAACAU UAA CCAUTT-3, 5-AUGGUUAAUGUUUGCAGGCTT-3; and scramble siRNA: 5-UUCUCCGAACGUGUCACGUTT-3, 5-ACGUGACACGUU CGGAGAATT-3.

Western Blot and Real-Time PCR

Western blot and real-time PCR were performed as previously described [28]. Briefly, cells were lysed, and the lysate was loaded onto 10% SDS-PAGE and then transferred to PVDF membranes (Millipore, Billerica, MA, USA). The membranes were blocked in 5% fat-free milk for 2 hours and subsequently incubated with different primary antibodies at 4°C overnight. Detailed information regarding the primary antibodies is listed in Supporting Information Table S1. Quantitative analysis of the Western blot was carried out using ImageJ software. Relative protein levels were quantified as the ratio of the level of target protein to the level of β-actin, in each group. Total RNA from cultured cells was extracted using Trizol reagent (Vazyme, Nanjing, Jiangsu, China) according to the manufacturer's instructions. Quantitative real-time PCR analyses were performed in triplicate using SYBR Green PCR Master Mix (TaKaRa), and reactions were detected using an Applied Biosystems 7300 Real-time PCR system (Applied Biosystems, Gaithersburg, CA, USA). The primer sequences used for real-time PCR are listed in Supporting Information Table S2.

Chromatin Immunoprecipitation

Chromatin immunoprecipitation (ChIP) analysis was carried out using EZ-ChIP (Millipore) according to the manufacturer's protocol. Briefly, FD BMSCs were crosslinked with fresh 1% formaldehyde; subsequently, the cells were lysed in SDS buffer and sonicated to shear the DNA. Lysates diluted with ChIP dilution buffer were immunoprecipitated with anti-CREB1 or anti-H3K9Ac (CST, Danvers, Chicago, USA) and rabbit IgG was used as an internal control. Reverse-crosslinked DNA was transferred to real-time PCR analysis. Detailed information, including the primer sequences used for real-time PCR, is listed in Supporting Information Table S3.

Dual Luciferase Reporter Assay

The putative binding region of CREB1 in the human *HDAC8* promoter was amplified by PCR from genomic DNA and cloned downstream of the firefly luciferase gene (FL) in the pGL3-basic luciferase reporter vector (Genecopoeia, Guangzhou, Guangdong, China). For luciferase reporter assays, 293T cells were co-transfected with individual pGL3-HDAC8 reporter plasmids and LeV-CREB1 plasmids using lipofectamine 2000. At 48 hours post-transfection, cells lysates were collected and assayed with a Dual-Luciferase Assay kit (Promega, Madison, WI, USA) following the manufacturer's instructions. The pRL Renilla luciferase (RL) reporter was used for data normalization. Results are displayed as the ratio of FL/RL activity.

In Vivo Therapeutic Animal Model

All animal procedures were performed according to the guidelines of the Institutional Animal Care and Use Committee of Nanjing Medical University (IACUC 1601016). Approximately 5×10^6 cells were attached to each HA/TCP biomaterial (Φ 6 × H 2 mm, Sichuan University, Chengdu, Sichuan, China). After 12 hours, the complexes were implanted subcutaneously into the backs of 7-week-old athymic nude mice (BALB/C, female, *n* = 6 per group, Vital River Laboratory Animal Technology Co. Beijing, China). The mice were allocated randomly into cages and were housed 4–5 animals per cage in standard cages at 25°C with unlimited rodent chow and water. To investigate the effects of *HDAC8*-selective inhibition on the osteogenic differentiation of FD BMSCs in vivo, the mice were randomly assigned to receive either vehicle control or PCI-34051 (20 mg/kg per day; Selleck, Houston, TX, USA). PCI-34051 was dissolved in 5% DMSO (Sigma) and 95% PBS and was administered via i.p. injection daily, 5 days/week for 2 weeks. Eight weeks after implantation, samples were harvested

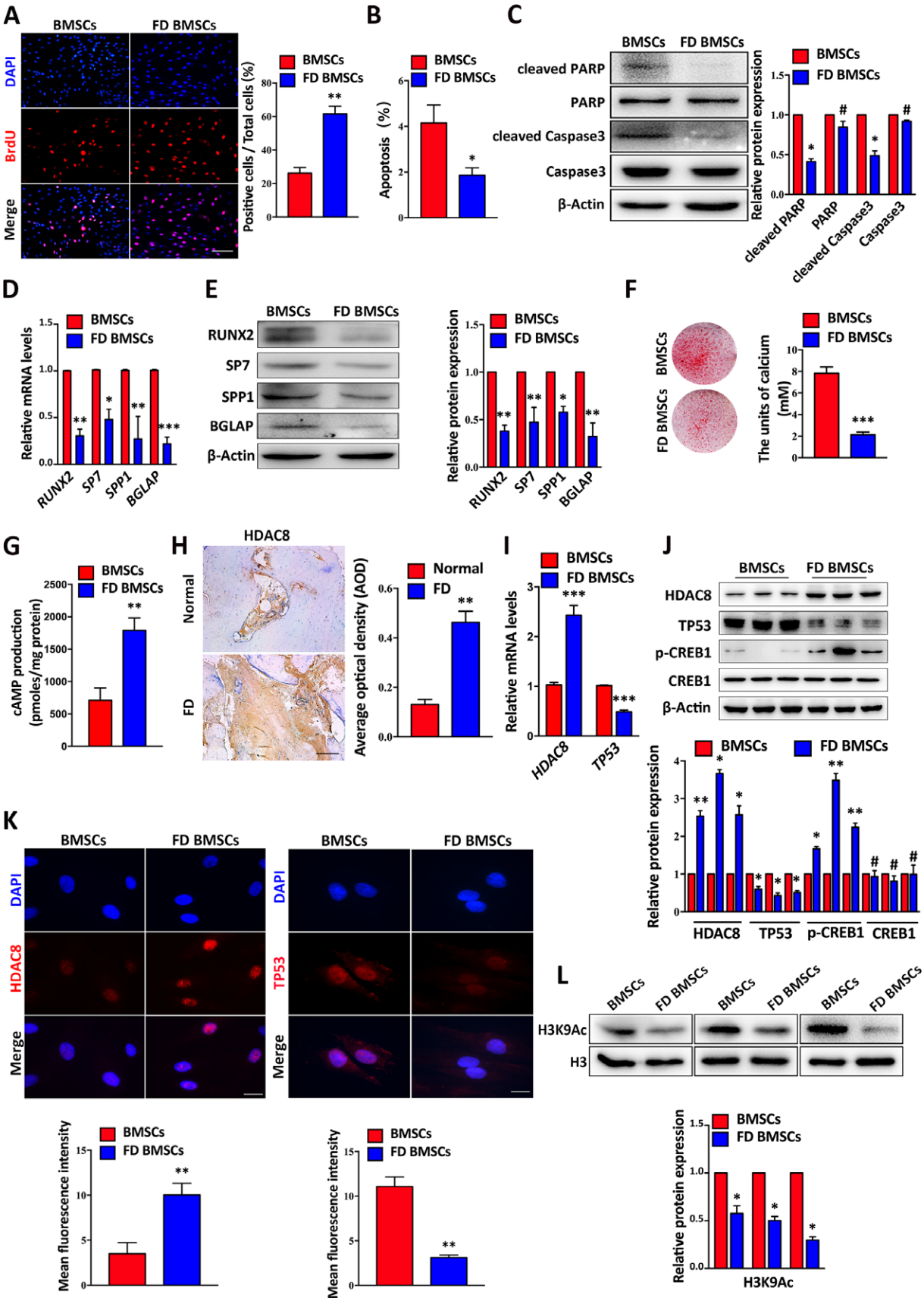

Figure 1. *(Legend appears on next page.)*

for histologic staining. Quantification of bone matrix in the sections stained with H&E and Masson trichrome was performed with ImageJ software. The results were expressed as a percentage of mineralized volume fraction (bone volume/total volume, BV/TV). For the quantification of immunohistochemistry, the total integral optical density was examined by ImageJ and then divided by the total measurement area. Finally, the results were shown as average optical density.

Statistical Analysis

All data examined are expressed as the mean ± SEM. All in vitro experiments were repeated independently at least three times. The statistical significance between groups was calculated using Student's *t* test. *p*-value < .05 (two sided) was considered significant.

RESULTS

Cytological Features of BMSCs from Craniofacial FD Lesions

The results of the *GNAS* mutation analysis are shown in Supporting Information Table S4. A mutation in the Gsα codon of Arg201 was found in 34 of the 42 (81%) cases of FD, with a predilection for Arg-to-His (R201H) substitutions (25 cases, 74%) versus Arg-to-Cys (R201C) substitutions (nine cases, 26%). The representative radiologic examination, clinicopathological features, and *GNAS* mutations of craniofacial FD patients were showed in Supporting Information Figure S1A–1C. As the histological results, BMSCs from FD lesions carried the specific *GNAS* mutations (Supporting Information Fig. S1D). No obvious morphologic differences between FD BMSCs and normal BMSCs were observed (Supporting Information Fig. S1E). However, FD BMSCs exhibited stronger proliferation ability and weaker apoptosis relative to BMSCs (Fig. 1A–1C). Next, we investigated the osteogenic potential of FD BMSCs and observed that the expression of osteogenic markers and calcification were downregulated in FD BMSCs during osteogenic induction (Fig. 1D–1F). The ELISA assays indicated that cAMP levels of FD BMSCs were significantly enhanced compared with normal BMSCs (Fig. 1G). To investigate whether *HDAC8* is associated with the impaired osteogenesis of FD BMSCs, *HDAC8* expression in FD tissue and FD BMSCs was examined. Increased *HDAC8* expression was found in FD histological sections (Fig. 1H). There was significantly higher *HDAC8* expression in FD BMSCs than in control cells (Fig. 1I, 1J) and no obvious increased expression of other HDACs was detected (Supporting Information Fig. S1F). As expected, phosphorylated CREB1 (p-CREB1) was also highly expressed in FD BMSCs (Fig. 1J). The localization of *HDAC8*, visualized by immunofluorescence, was consistent with these results (Fig. 1K). In addition, the expression of *TP53*, an important factor that regulates cellular apoptosis, was detected (Fig. 1I–1K). Furthermore, there was significantly lower H3K9Ac expression in FD BMSCs than in normal BMSCs (Fig. 1L). These results indicate that *HDAC8* and H3K9Ac may participate in the regulation of the osteogenic differentiation of FD BMSCs, and the ability to suppress apoptosis is likely related to *TP53* downregulation.

In Vitro, BMSCs Treated with Exogenous cAMP Show Similar Characteristics to FD BMSCs, and cAMP Inhibition Improves the Properties of FD BMSCs

Based on the above observations, we hypothesized that *HDAC8* upregulation and *TP53* downregulation may be mediated by high cAMP expression in FD BMSCs. Therefore, we used a cellular model to imitate the pathological process of FD BMSCs: normal BMSCs treated with exogenous cAMP. Dibutyryl cAMP (cAMP) remarkably increased intracellular cAMP expression (Supporting Information Fig. S2A). As the properties of FD BMSCs, *HDAC8*, and *TP53* expression in normal BMSCs treated with cAMP were significantly different with control (Fig. 2A, 2B). However, increased expression of other HDACs was less apparent than *HDAC8* (Supporting Information Fig. S2B). Importantly, BMSCs with ectopic cAMP expression exhibited similar properties to FD BMSCs (Fig. 2C–2H). In addition, a previous research examined the inhibition of basal cAMP production by bupivacaine [29]. In this study, the downregulation of basal cAMP production due to bupivacaine HCl (Bupivacaine) was presented in Supporting Information Figure S2C. We firstly evaluated the gene expression of *HDAC8* and *TP53* in two groups treated with either DMSO or Bupivacaine. Although reduce in the expression of other HDACs was less apparent than *HDAC8* (Supporting Information Fig. S2D), a larger decrease in the expression of *HDAC8* in Bupivacaine-treated FD BMSCs was observed (Fig. 2I, 2J). Interestingly, as we detected opposing results for *TP53* expression, *TP53* levels were upregulated in response to Bupivacaine treatment (Fig. 2I, 2J). These results confirm that *HDAC8* and *TP53* are downstream genes of cAMP. To further investigate the role of cAMP downregulation in FD BMSCs, as illustrated in Figure 2K–2P, these results suggest that the enhanced proliferation and impaired

Figure 1. Biological characteristics of FD BMSCs. **(A):** Representative BrdU incorporation in FD BMSCs. Scale bar, 100 μm. **(B):** Apoptotic assays showed the apoptosis of FD BMSCs. **(C):** The protein expression of cleaved PARP and cleaved Caspase3 was lower in FD BMSCs than that in normal BMSCs. Relative protein levels were quantified as the ratio of the level of cleaved PARP to the level of PARP (cleaved Caspase3 to total Caspase3). All the other gray values were normalized to β-actin. **(D):** Real-time PCR analysis of osteogenesis marker mRNA expression in FD BMSCs after osteogenic induction for 7 days. **(E):** Western blot analysis of osteogenesis markers of FD BMSCs cultured with osteogenesis induction medium for 7 days. **(F):** After 14 days osteogenic induction, Alizarin Red staining showed decreased deposition of calcium in FD BMSCs. **(G):** cAMP levels in FD BMSCs and control cells were analyzed by ELISA. **(H)**: Immunohistochemistry of *HDAC8* in the tissues from normal jaw and FD lesion. Scale bar, 200 μm. **(I)**: Real-time PCR was used to detect *HDAC8* and *TP53* mRNA expression. **(J):** Western blot: *HDAC8*, TP53, p-CREB1, and CREB1 protein levels. For the expression of p-CREB1, relative protein levels were quantified as the ratio of the level of p-CREB1 to the level of CREB1. All the other gray values were normalized to β-actin. **(K):** Immunofluorescence of FD BMSCs exhibited increased HDAC8 expression and decreased *TP53* expression. ImageJ software was used for the quantification of mean fluorescence intensity of. Scale bar, 50 μm. **(L):** H3K9Ac protein level was detected by Western blot. Data are means ± SEM. #, $p > .05$; *, $p < .05$; **, $p < .01$; ***, $p < .001$. Abbreviations: *BGLAP*, bone gamma-carboxyglutamic acid-containing protein; BMSCs, bone marrow stromal cells; CREB1, cAMP-response element binding protein 1; FD, fibrous dysplasia; H3, histone 3; H3K9Ac, acetylation of H3 at Lys9; *HDAC8*, histone deacetylase 8; p-CREB1, phosphorylated CREB1; PARP, poly ADP-ribose polymerase; *RUNX2*, runt-related transcription factor 2; *SP7*, special protein 7; SPP1, secreted phosphoprotein 1; *TP53*, tumor protein 53.

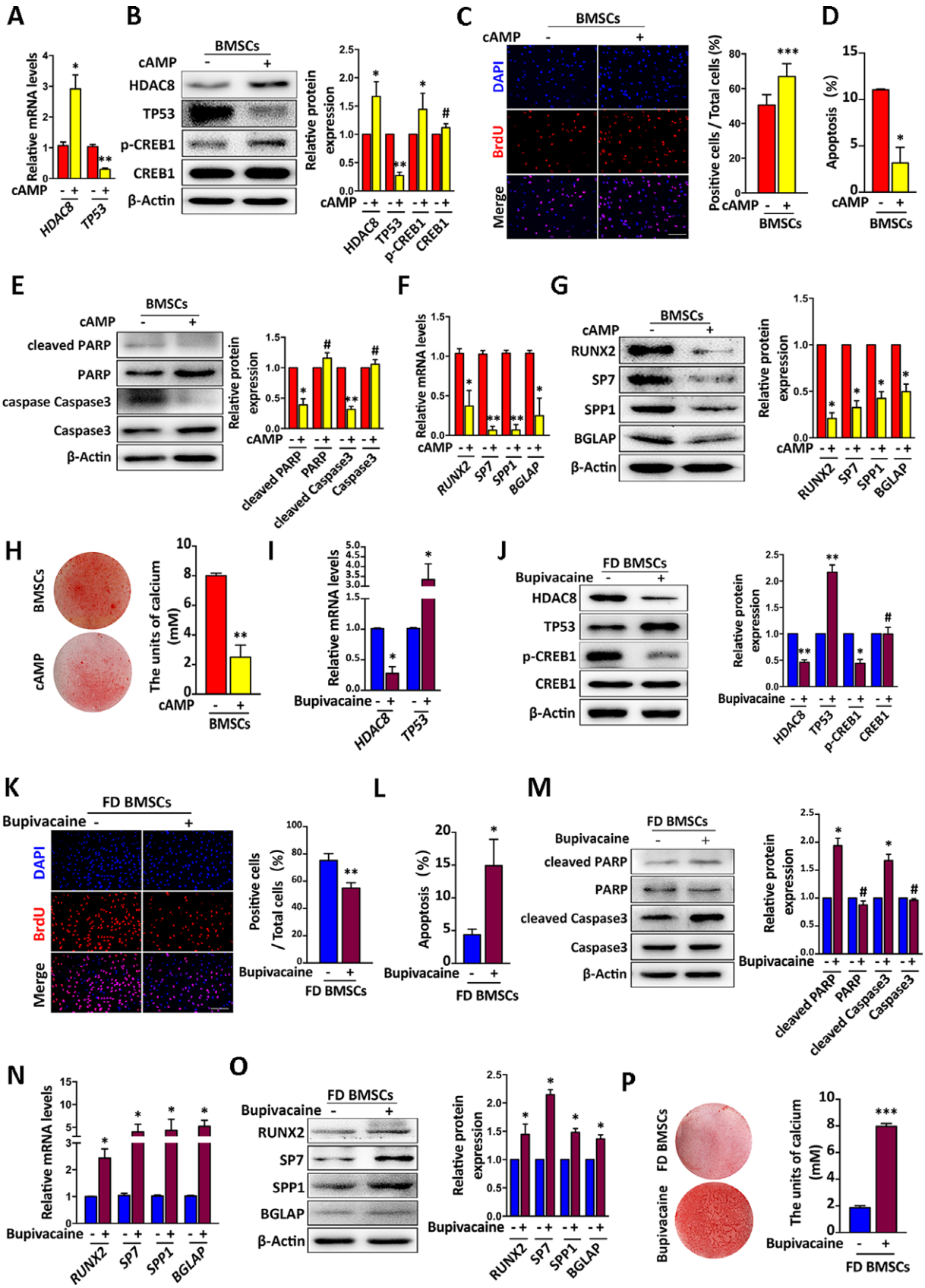

Figure 2. *(Legend appears on next page.)*

osteogenesis potential of FD BMSCs are able to be considerably recovered through cAMP inhibition.

HDAC8 Inhibition or Knockdown Prevents the Pathological Characteristics of FD BMSCs

To determine whether *HDAC8* directly regulates the properties of FD BMSCs, the specific *HDAC8* inhibitor PCI-34051 was used to treat FD BMSCs to investigate changes in FD BMSCs following *HDAC8* downregulation. After the pretesting study, 15 μM was selected as the appropriate concentration of PCI-34051 for treating FD BMSCs (Supporting Information Fig. S3A, 3B). Prominently increased *TP53* expression was observed in FD BMSCs treated by PCI-34051 with 15 μM for 48 hours (Fig. 3A, 3B) and the level of H3K9Ac was increased with use of PCI-34051 (Fig. 3B). Diminished BrdU incorporation was detected in cells treated with PCI-34051 for 12 hours compared with control cells (Fig. 3C). Furthermore, the population of apoptotic cells was significantly increased in FD BMSCs after *HDAC8* inhibition (Fig. 3D). The expression of cleaved PARP and cleaved Caspase3 was higher in FD BMSCs treated with PCI-34051 for 48 hours than that in the control (Fig. 3E). FD BMSCs treated with PCI-34051 exhibited increased expression of osteogenic markers and increased calcium deposition formation after osteogenic induction (Fig. 3F–3H). In addition, to verify whether *HDAC8* mRNA silencing could modify the properties of FD BMSCs, an exogenous shHDAC8 expression lentivirus (LeV-shHDAC8) was introduced into FD BMSCs. The LeV-shHDAC8-1 was selected for the subsequent research because of its highest efficiency in three LeV-shHDAC8 sequences (Fig. 3I). First, *TP53* upregulation were observed in FD BMSCs transfected with LeV-shHDAC8 (Fig. 3J). Second, transfection with LeV-shHDAC8 remarkably ameliorated the biological characteristics and functions of FD BMSCs, corresponding to *HDAC8* inhibition (Fig. 3K–3P). Therefore, we preliminarily consider that *HDAC8*, as the upstream gene of *TP53*, plays an important role in the abnormal phenotypes of FD BMSCs via H3K9Ac.

CREB1 Binds the CRE in HDAC8 Promoter to Enhance Its Transcription in FD BMSCs

Our study has shown that the expression of *HDAC8* significantly decreased with the inhibition of cAMP production in FD BMSCs. In addition, exogenous cAMP could upregulate the expression of *HDAC8* in normal BMSCs as previously described. However, no evidence has yet been found for the detailed molecular mechanisms underlying the regulatory roles of CREB on *HDAC8*. Thus, we screened the *HDAC8* promoter region and observed that CREB1 might bind to five putative binding sites (CREs) in the region from −1,996 to −408 bp. To test the existence of cAMP-CREB1-HDAC8 axis, three CREB1-targeting siRNA sequences were synthesized, and si-CREB1-1 was selected for the further research (Fig. 4A). Following CREB1-targeting RNAi there was a significant reduction in *HDAC8* expression and an evident increase in *TP53* expression after CREB1 silencing (Fig. 4B, 4C).

To confirm that CREB1 could physically bind to the promoter of *HDAC8* and promote its transcription in FD BMSCs, we performed ChIP assays with a specific anti-CREB1 construct and five primers covering the *HDAC8* promoter region. Significant enrichment of CREB1 was observed at four putative binding sites in the *HDAC8* promoter region (Fig. 4D). To further verify the regulatory function of CREB1 binding in *HDAC8* transcription, we constructed *HDAC8* luciferase reporters that contained the four binding sites (vector1 containing site1, vector2 containing site3, and vector3 containing site4 and 5). These reporters were co-transfected with the human CREB1 plasmid into 293T cells. Results from luciferase reporter assays indicated that the luciferase activity was significantly increased in cells with the reporters containing binding site 1 or 3, while the luciferase activity in cells containing the fourth and fifth binding site was comparable to that of the control (Fig. 4E). Collectively, these findings indicate that CREB1 promotes *HDAC8* transcription by directly binding to its promoter region in FD BMSCs.

Moreover, directly regulation of CREB1 to the promoter of *RUNX2* and *TP53* were also detected by ChIP assays (Fig. 4F). It suggested that CREB1 possibly promoted the transcription of *RUNX2* and *TP53* in FD BMSCs. Besides, the promoter region of both *RUNX2* and *TP53* contained H3K9Ac were reflected (Fig. 4G). Based on this, upregulated HDAC8 in FD BMSCs could induce a lower H3K9 acetylation level of promoter region of *RUNX2* and *TP53* and subsequently suppressed their expression. Compared to the activation of *RUNX2* and *TP53* mediated by CREB1, the inactivation of *RUNX2* and *TP53* caused by excessive *HDAC8* may be dominant in FD BMSCs.

Figure 2. A cell model to imitate the pathological process of FD BMSCs and the recovery of FD BMSC properties following cAMP inhibition. The expression levels of *HDAC8* and *TP53* with BMSCs treated with 2 mM cAMP for 48 hours were determined by **(A)** real-time PCR and **(B)** Western blot. **(C):** Representative images of BrdU-positive cells in BMSCs treated with 2 mM cAMP for 12 hours. Scale bar, 100 μm. **(D):** Apoptosis assays showed that cAMP downregulated the number of apoptotic cells of BMSCs. **(E):** The expression of cleaved PARP and cleaved Caspase3 decreased in BMSCs treated with cAMP. The expression levels of osteogenesis markers decreased in BMSCs treated with 2 mM cAMP for 7 days by **(F)** real-time PCR and **(G)** Western blot. **(H):** Alizarin Red staining was performed after 14 days osteogenic induction. Patterns of *HDAC8* and *TP53* mRNA expression in FD BMSCs treated with Bupivacaine (Bupivacaine HCl, 10 μM) for 48 hours were determined by **(I)** real-time PCR and **(J)** Western blot. **(K):** The proliferation of FD BMSCs treated with Bupivacaine for 12 hours was analyzed in a BrdU assay. **(L):** Apoptotic analysis of FD BMSCs treated with Bupivacaine for 12 hours was performed by FACS. **(M):** The protein expression of cleaved PARP and cleaved Caspase3 was higher in FD BMSCs treated with Bupivacaine for 48 hours than that in the control. The osteogenesis markers of two groups cells cultured in osteogenic medium for 7 days were analyzed by **(N)** real-time PCR and **(O)** Western blot. **(P):** The representative images of Alizarin Red staining were shown. All experiments were performed at least three times. $^{\#}$, $p > .05$; *, $p < .05$; **, $p < .01$; ***, $p < .001$. Abbreviations: *BGLAP*, bone gamma-carboxyglutamic acid-containing protein; BMSCs, bone marrow stromal cells; CREB1, cAMP-response element binding protein 1; FD, fibrous dysplasia; HDAC8, histone deacetylase 8; p-CREB1, phosphorylated CREB1; PARP, poly ADP-ribose polymerase; *RUNX2*, runt-related transcription factor 2; *SP7*, special protein 7; SPP1, secreted phosphoprotein 1; *TP53*, tumor protein 53.

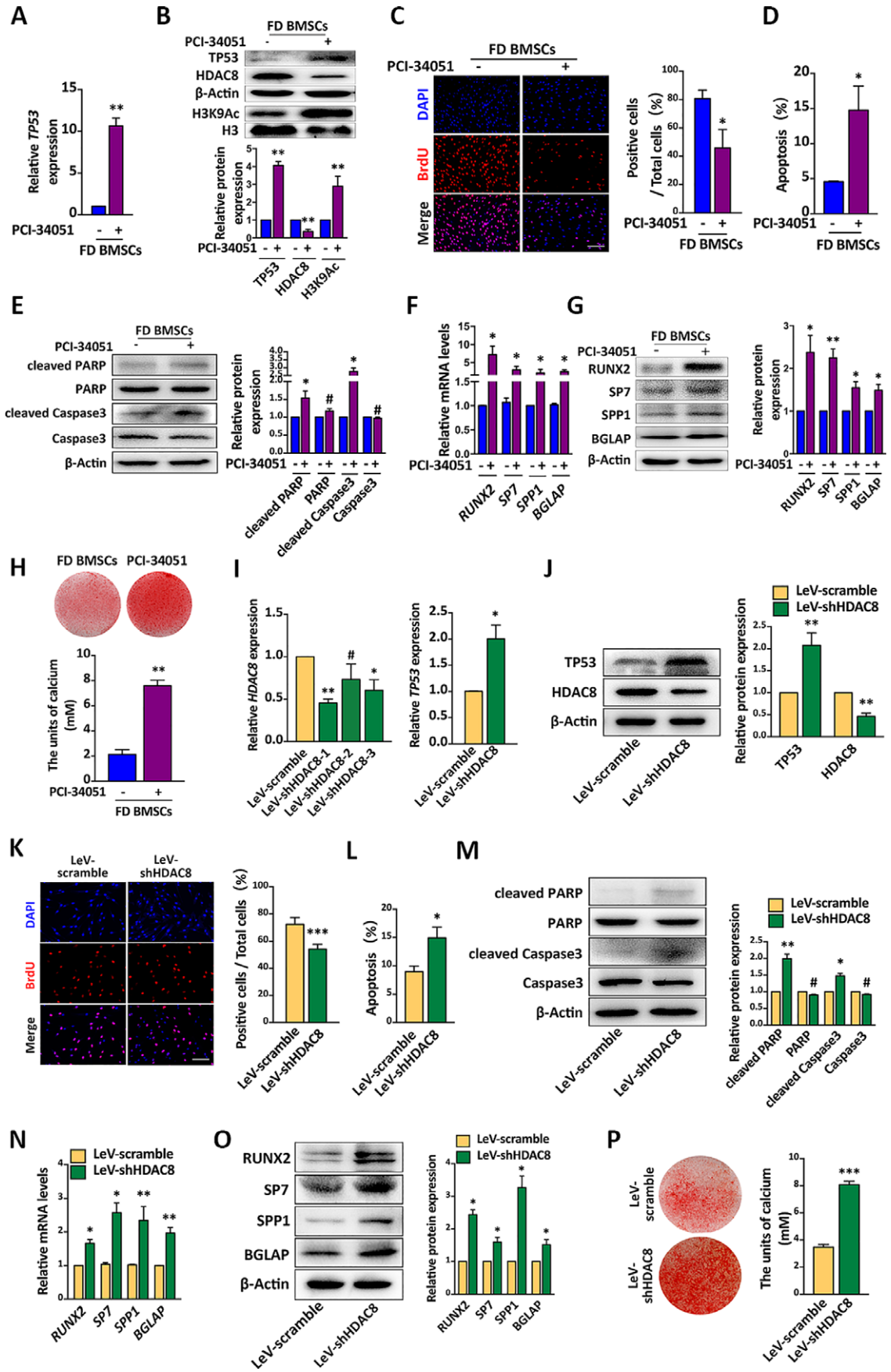

Figure 3. *(Legend appears on next page.)*

HDAC8 Inhibition or Knockdown Enhances the Osteogenesis Potential of FD BMSCs In Vivo

In light of the clear therapeutic potential of *HDAC8* inhibition, we examined ectopic bone formation in FD BMSCs treated with LeV-scramble, LeV-shHDAC8 and PCI-34051 in nude mice. We implanted HA/TCP scaffolds loaded with FD BMSCs into intramuscular pockets in nude mice (Fig. 5A). Eight weeks after implantation, we harvested the specimens and subjected them to histological examination. The organized bone matrix was formed in the *HDAC8*-knockdown group and the PCI-treated group, whereas there was a significant amount of fibrous tissue in the negative control (Fig. 5B). FD BMSCs treated with *HDAC8* downregulation induced more ectopic bone formation compared to the control groups. Then, the immunohistochemistry for *RUNX2* and bone gamma-carboxyglutamic acid-containing protein (*BGLAP*) was performed to evaluate osteoblastic activity. FD BMSCs treated with *HDAC8* knockdown or inhibition exhibited increased *RUNX2* and *BGLAP* expression (Fig. 5C). Thus, *HDAC8* downregulation could enhance the osteogenesis of FD BMSCs in vivo.

Discussion

FD is a stem cell disease of bone caused by activated *GNAS* mutations in BMSCs from FD lesions [30, 31]. *GNAS* mutation leads to increased transcription of several early immediate genes, including c-fos and c-jun, which seem to play a critical role in the control of FD BMSCs proliferation, via a cAMP-CREB pathway [22, 32]. However, the detailed mechanism that these genes regulate FD BMSCs proliferation is unclear, interestingly, we found that the apoptotic potential of FD BMSCs was weaker than that of normal BMSCs and there was a significant downregulation of *TP53* expression in FD BMSCs. Therefore, enhanced proliferation and reduced apoptosis might be associated with a lack of *TP53*.

We recently reported that *HDAC8* suppressed osteogenic differentiation of BMSCs. Although HDAC1–8 have the inhibitory roles in osteoblast differentiation via modulating histone acetylation or interacting with RUNX2 [21], we found that, in this study, only *HDAC8* expression was aberrantly increased among the HDACs in FD BMSCs. Therefore, based on our previous study and current results, we infer that high expression of *HDAC8* with low expression of H3K9Ac leads to the impaired osteogenic potential of FD BMSCs. Furthermore, this inhibitory effect may be caused by epigenetic regulation of *RUNX2* via HDAC8-mediated deacetylation of H3K9.

In addition, according to a previous report, *HDAC8* promotes proliferation and inhibits apoptosis and has been verified to suppress the production of *TP53* [25]. Furthermore, we identified *HDAC8* as an inhibitory effector of *TP53* in FD BMSCs based on the following evidence. Significantly increased *TP53* expression was observed in FD BMSCs treated with an *HDAC8* inhibitor or following *HDAC8* knockdown. Thus, *HDAC8* overexpression may lead to *TP53* downregulation, resulting in the weaker apoptosis of FD BMSCs. The detailed regulatory mechanism exerted by *HDAC8* on *TP53* in FD BMSCs is not yet clear, but our results indicate that *HDAC8* possibly inhibits the expression of *TP53* by regulating the level of H3K9Ac in the promoter regions of *TP53*. Here, we are unable to rule out the inhibitory effects of cAMP on *TP53* [23, 33], but we have shown that *HDAC8* can partially inhibit the expression of *TP53*.

cAMP activation and phosphorylation of CREB in osteoblasts play important roles in skeletal development by regulating osteoblast differentiation [34–36]. Additionally, CREB, acting as a potent trans-activating factor, promotes gene transcription although p-CREB binding to the promoter regions of target genes. However, previous studies have rarely examined the detailed effects of CREB on osteogenic differentiation or the impact of this transcription factor on FD BMSCs. To determine whether *HDAC8* is regulated by CREB, we firstly verified that *HDAC8* is the downstream effector of CREB. We further analyzed the promoter region of *HDAC8* and identified four putative binding sites of CREB1. Here, we proved the presence of cAMP-CREB1-HDAC8 axis, which is critically involved in the abnormal properties of FD BMSCs. However, given the complex roles of cAMP-CREB signaling in diverse settings [9, 37], we are unable to rule out the possibility that other downstream mediators of cAMP-CREB signaling in addition to *HDAC8* are involved. In the present study, we observed that CREB1 possibly promoted the transcription of *RUNX2* and *TP53* in FD BMSCs. Meanwhile, the promoter region of both *RUNX2* and *TP53* contained H3K9Ac was detected. Because of the low expression of H3K9Ac in FD BMSCs and increased H3K9Ac expression in FD BMSCs with *HDAC8* inhibitor treatment, we inferred *HDAC8* regulated expression of *RUNX2* and *TP53* via deacetylation of H3K9 in FD BMSCs. Compared to the activation of *RUNX2* and *TP53* mediated by CREB1, we thought that inactivation of *RUNX2* and *TP53* caused by *HDAC8* might be dominant in FD BMSCs. Interestingly, *HDAC8* resulted in decreased CREB activation and CREB mediated gene transcription in response to forskolin application [38]. We attributed this phenomenon to two possible reasons: first, upregulated HDAC8 might have different effects on CREB in different cell types; second, forskolin application might not utterly reflect the pathological overproduction of cAMP in FD BMSCs. Although

Figure 3. *HDAC8* silencing by inhibition or transfection reversed the characteristics of FD BMSCs. **(A):** Real-time PCR to detect TP53 mRNA expression in FD BMSCs treated with PCI-34051 (15 μM) for 48 hours. **(B):** Western blot analysis of *HDAC8*, *TP53*, and H3K9Ac in FD BMSCs treated with PCI-34051 for 48 hours compared with the control. **(C):** Cell proliferation was assessed in a BrdU assay. Scale bar, 100 μm. **(D):** Apoptotic analysis of FD BMSCs treated with *HDAC8* inhibitor for 12 hours. **(E):** FD BMSCs treated with PCI-34051 for 48 hours exhibited higher expression of cleaved PARP and cleaved Caspase3 than that in the control. The levels of osteogenesis markers of two group cells induced for 7 days were analyzed by **(F)** real-time PCR and **(G)** Western blot. **(H):** Alizarin Red staining showed that the PCI-34051 treatment group formed more calcium deposition. The analysis of *HDAC8* and *TP53* expression in FD BMSCs with LeV-shHDAC8 compared with the control (LeV-scramble) was performed by **(I)** real-time PCR and **(J)** Western blot. **(K):** BrdU incorporation assays were used to detect cell proliferation. Scale bar, 100 μm. **(L):** Greater numbers of apoptotic cells were observed in FD BMSCs transfected with LeV-shHDAC8. **(M):** The protein expression of cleaved PARP and cleaved Caspase3 in FD BMSCs with LeV-shHDAC8 was shown. Osteogenesis markers were analyzed by **(N)** real-time PCR and **(O)** Western blot. **(P):** Alizarin Red staining. All experiments were performed at least three times. $^{\#}$, $p > .05$; *, $p < .05$; **, $p < .01$; ***, $p < .001$. Abbreviations: *BGLAP*, bone gamma-carboxyglutamic acid-containing protein; BMSCs, bone marrow stromal cells; FD, fibrous dysplasia; H3, histone 3; H3K9Ac, acetylation of H3 at Lys9; *HDAC8*, histone deacetylase 8; PARP, poly ADP-ribose polymerase; RUNX2, runt-related transcription factor 2; *SP7*, special protein 7; SPP1, secreted phosphoprotein 1; *TP53*, tumor protein 53.

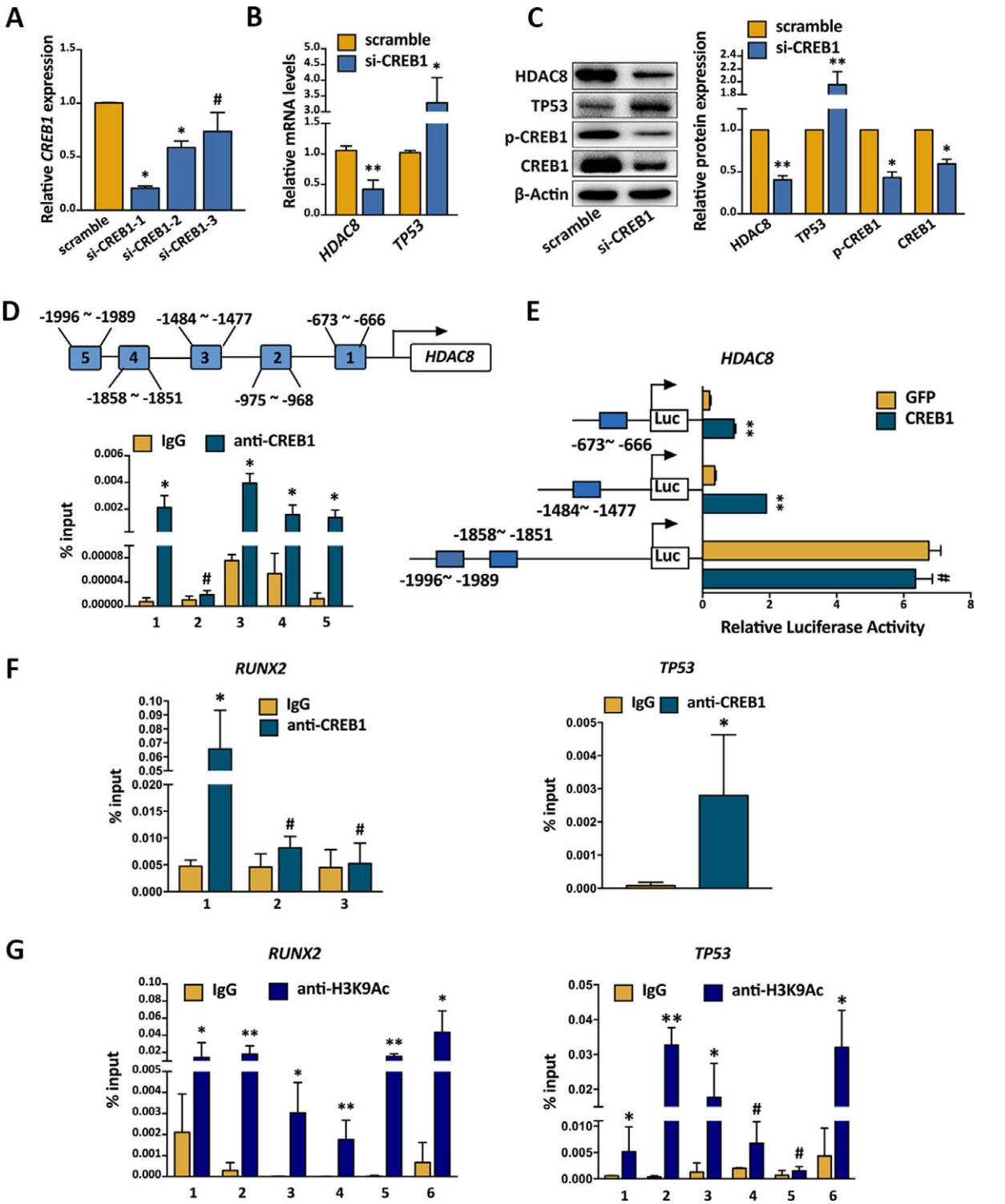

Figure 4. The specific mechanism by which cAMP promotes HDAC8 transcription in FD BMSCs. **(A):** The interference efficiency of three si-CREB1 sequences was detected by real-time PCR. **(B):** After si-CREB1 interference for 48 hours, representative real-time PCR analysis of *HDAC8* and *TP53* in FD BMSCs. **(C):** Western blot analysis of *HDAC8*, *TP53*, p-CREB1, and CREB1 protein levels in FD BMSCs transfected with si-CREB1 for 72 hours. **(D):** Five primers were designed to cover the human *HDAC8* promoter region and were used to identify CREB1 binding sites in a ChIP assay. Four putative CREB1 binding sites in the *HDAC8* promoter region were identified. **(E):** Luciferase reporter assays indicated that the luciferase activity was significantly increased in cells containing the reporters with binding site1 (−673 to −666 bp) or binding site3 (−1,484 to −1,477 bp) in *HDAC8* promoter region; the results showed no statistically significant increase of luciferase activity in the reporter with binding site4 (−1,858 to −1,851 bp) and binding site5 (−1,996 to −1,989 bp). **(F):** ChIP assays showed one putative CREB1 binding site in either *RUNX2* or *TP53* promoter region. **(G):** Six putative H3K9Ac binding sites in *RUNX2* and four putative H3K9Ac binding sites in *TP53* promoter region were identified by ChIP. $N \geq 3$. #, $p > .05$; *, $p < .05$; **, $p < .01$. Abbreviations: CREB1, cAMP-response element binding protein 1; H3K9Ac, acetylation of H3 at Lys9; *HDAC8*, histone deacetylase 8; p-CREB1, phosphorylated CREB1; si-CREB1, small interfering RNA targeting CREB1; *TP53*, tumor protein 53.

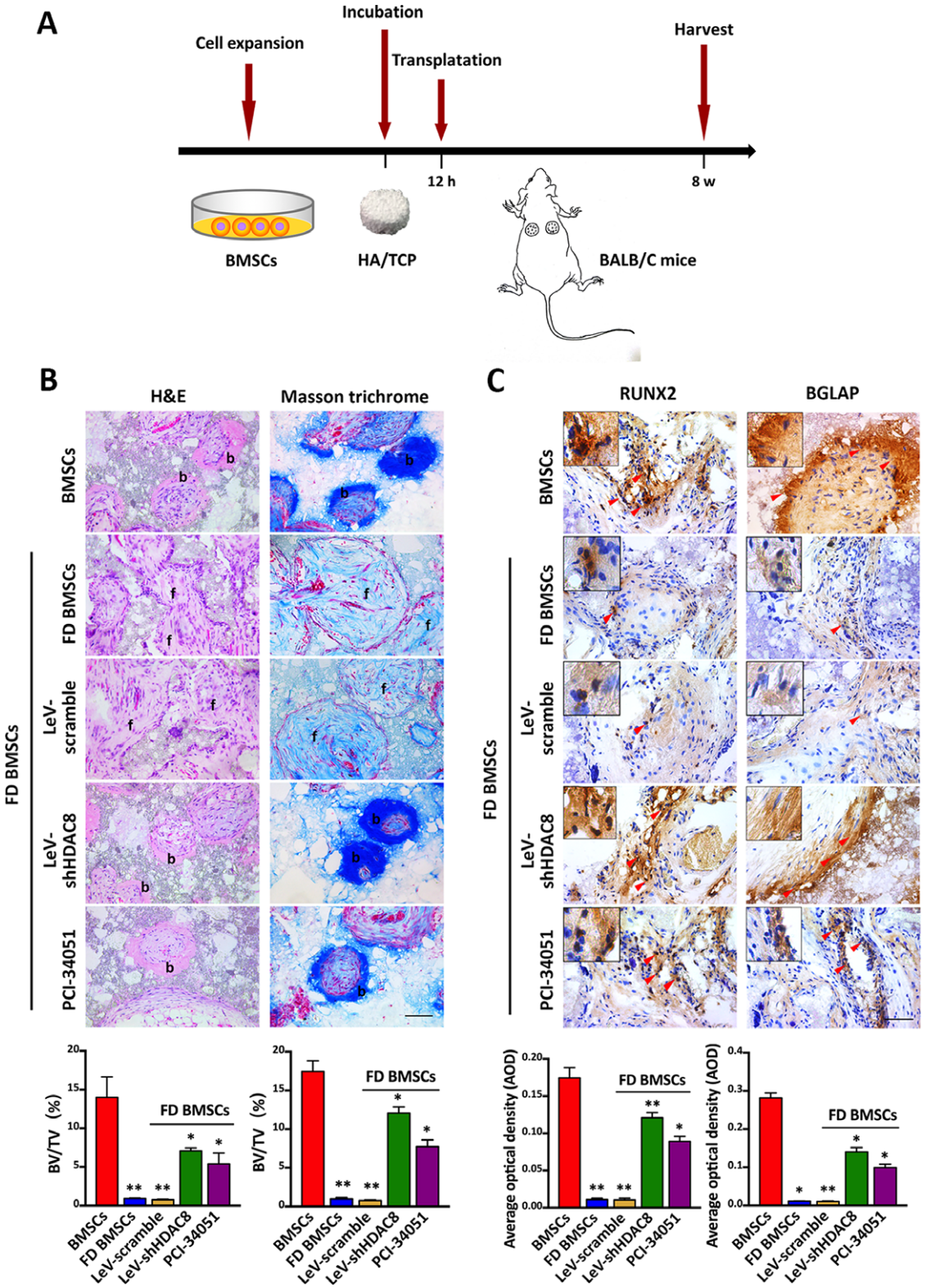

Figure 5. *HDAC8* inhibition or knockdown enhanced the osteogenesis potential of FD BMSCs in vivo. **(A):** HA/TCP scaffolds loaded with FD BMSCs were implanted into the intramuscular pockets of the backs of nude mice. Complexes from different groups were transplanted into both sides of the backs of nude mice. *N* = 6 per group. Eight weeks later, the complexes were harvested, decalcified, and embedded in paraffin and stained with H&E and Masson trichrome **(B)**, scale bar, 100 μm; and immunohistochemistry of RUNX2 and *BGLAP* **(C)**, Scale bar, 100 μm. b: bone; f: fibrotic tissue; red arrowhead indicated the positive staining. *, $p < .05$; **, $p < .01$. Abbreviations: AOD, average optical density; *BGLAP*, bone gamma-carboxyglutamic acid-containing protein; BMSCs, bone marrow stromal cells; BV, bone volume; FD, fibrous dysplasia; RUNX2, runt-related transcription factor 2; TV, total volume.

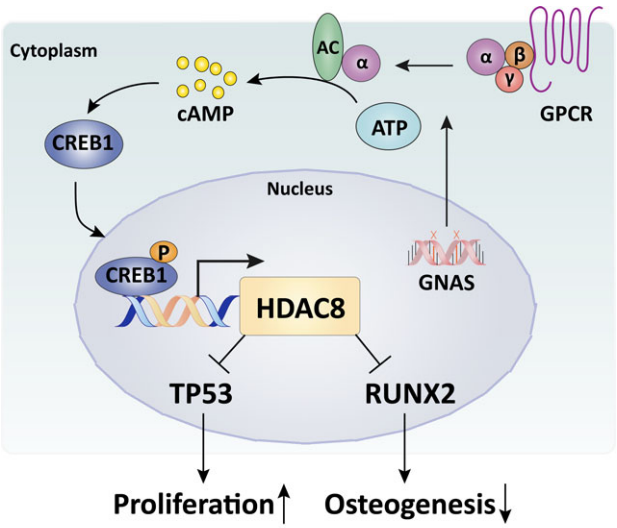

Figure 6. The cAMP-CREB1-HDAC8 axis in BMSCs from FD lesions. *GNAS* mutation leads to increased stimulation of AC and the overproduction of cAMP. In response to cAMP overproduction, phosphorylated CREB1 translocates into the nucleus and binds to the CRE of the *HDAC8* promoter to activate its transcription. Upregulation of *HDAC8* leads to enhanced proliferation and decreased osteogenesis caused by its inhibitory effects of the activation and transcription of *RUNX2* and the pro-apoptotic ability of *TP53*. Abbreviations: AC, adenylyl cyclase; ATP, adenosine triphosphate; CREB1, cAMP-response element binding protein 1; *GNAS*, guanine nucleotide-binding protein alpha-stimulating activity polypeptide; GPCR, guanosine-binding protein coupled receptor; *HDAC8*, histone deacetylase 8; RUNX2, runt-related transcription factor 2; *TP53*, tumor protein 53.

we could not negate completely for the inactivation of CREB mediated by upregulated *HDAC8*, compared to the inactivation of CREB mediated by HDAC8, the activation of CREB caused by excessive cAMP may be dominant in FD BMSCs based on our results.

To date, clinical medical treatments for FD are still mainly focused on relieving symptoms [4]. The efficacy of antiresorptive agents such as bisphosphonates and denosumab is limited, and no studies have verified their apparent benefit from a long-term follow-up perspective [39, 40]. In our report, several potential therapeutic interventions may be used to target the cAMP-CREB1-HDAC8 pathway, and HDAC8 may also be a potential and important therapeutic target. Recent evidence indicates that HDAC inhibition enhances cell differentiation in vivo [41–43], and more importantly HDAC8-selective targeting has been identified to be effective in several diseases [44, 45]. In this study, PCI-34051, an HDAC8-specific inhibitor [46], was used to study the role of HDAC8 intervention in nude mice implanted with FD BMSCs. Here, we verify the small-molecule inhibition of HDAC8 as a novel and alternative therapeutic strategy that is preliminarily effective for improving the impaired differentiation potential of FD BMSCs in vivo. However, its application in clinical practice requires further study to clarify the value of HDAC8 as a novel therapeutic target in FD. This issue may be addressed by constructing a better animal model of FD [47–49] and by examining the drug metabolism and pharmacokinetics of HDAC8-specific inhibitors. Recent research appeared that a conditional tetracycline-inducible animal model expressing the $G\alpha_s^{R201C}$ in the skeletal stem cell linage was established and represented FD-like bone lesions [49]. In the present study, we used HA/TCP scaffold as carrier of cells to perform vivo research, and the effectiveness of ectopic bone formation was revealed. HA/TCP scaffold, a kind of widely used bioceramic materials, is applied to bone and dental tissue engineering [50]. The scaffold could provide suitable space for cellular attachment and homing [51]. Duing to the similar chemical structures to bone and teeth, HA/TCP is appropriate for bone and dental grafting [52]. However, there still have limitations to used HA/TCP scaffolds as models to reflect systemic condition of FD and further more appropriate animal models still needed.

In summary, our studies, taken together with these results, demonstrate for the first time that the cAMP-CREB1-HDAC8 axis is strongly associated with the disordered properties of FD BMSCs (Fig. 6). Furthermore, intervention of the cAMP-CREB1-HDAC8 pathway reverses the FD phenotype to some degree. Importantly, this study provides useful insights into the molecular pathogenesis of FD and the evaluation of novel therapeutic options for FD in vitro and in vivo.

Conclusion

The current study demonstrates that cAMP-CREB1-HDAC8 pathway participates in maintaining the pathological phenotype in FD BMSCs. Our study goes further to explore the therapeutic effect of PCI-34051 (a small molecule inhibitor targeting *HDAC8*) in FD BMSCs. In this context, our results suggest that targeted modulation of *HDAC8* in FD BMSCs might be a potential therapeutic strategy for FD in vitro and in vivo. Continued pursuit of this pathway may be hopeful to provide a possible strategy for FD patients.

Acknowledgments

This work was supported by National Natural Science Foundation of China Grant (81500874) and a project funded by the Priority Academic Program for the Development of Jiangsu Higher Education Institutions (2014-37).

Author Contributions

T.X.: conception and design, performed research, data analysis and interpretation, manuscript writing; Y.F.: conception and design, data analysis and interpretation; W.Z.: performed research, data analysis and interpretation; R.X., L.X., Y.D.: collection and/or assembly of data; P.Z.: performed research; J.C.: provision of study material or patients; H.J.: conception and design, provision of study material or patients.

Disclosure of Potential Conflicts of Interest

The authors indicated no potential conflicts of interest.

References

1 Khan SK, Yadav PS, Elliott G et al. Induced Gnas(R201H) expression from the endogenous Gnas locus causes fibrous dysplasia by up-regulating Wnt/beta-catenin signaling. Proc Natl Acad Sci USA 2018;115: E418–E427.

2 Akintoye SO, Boyce AM, Collins MT. Dental perspectives in fibrous dysplasia and McCune-Albright syndrome. Oral Surg Oral Med Oral Pathol Oral Radiol 2013;116:e149–e155.

3 Zhou SH, Yang WJ, Liu SW et al. Gene expression profiling of craniofacial fibrous dysplasia reveals ADAMTS2 overexpression as a potential marker. Int J Clin Exp Pathol 2014; 7:8532–8541.

4 Faruqi T, Dhawan N, Bahl J et al. Molecular, phenotypic aspects and therapeutic horizons of rare genetic bone disorders. Biomed Res Int 2014;2014:670842.

5 Feller L, Wood NH, Khammissa RA et al. The nature of fibrous dysplasia. Head Face Med 2009;5:22.

6 Robey PG, Kuznetsov S, Riminucci M et al. The role of stem cells in fibrous dysplasia of bone and the Mccune-Albright syndrome. Pediatr Endocrinol Rev 2007;4(Suppl 4):386–394.

7 Zhang S, Kaplan FS, Shore EM. Different roles of *GNAS* and cAMP signaling during early and late stages of osteogenic differentiation. Horm Metab Res 2012;44:724–731.

8 Riminucci M, Robey PG, Saggio I et al. Skeletal progenitors and the *GNAS* gene: Fibrous dysplasia of bone read through stem cells. J Mol Endocrinol 2010;45:355–364.

9 Sands WA, Palmer TM. Regulating gene transcription in response to cyclic AMP elevation. Cell Signal 2008;20:460–466.

10 Ionescu AM, Drissi H, Schwarz EM et al. CREB cooperates with BMP-stimulated Smad signaling to enhance transcription of the Smad6 promoter. J Cell Physiol 2004;198:428–440.

11 Mayr B, Montminy M. Transcriptional regulation by the phosphorylation-dependent factor CREB. Nat Rev Mol Cell Biol 2001;2: 599–609.

12 Fan QM, Yue B, Bian ZY et al. The CREB-Smad6-Runx2 axis contributes to the impaired osteogenesis potential of bone marrow stromal cells in fibrous dysplasia of bone. J Pathol 2012;228:45–55.

13 Lee HW, Suh JH, Kim AY et al. Histone deacetylase 1-mediated histone modification regulates osteoblast differentiation. Mol Endocrinol 2006;20:2432–2443.

14 Paino F, La Noce M, Tirino V et al. Histone deacetylase inhibition with valproic acid downregulates osteocalcin gene expression in human dental pulp stem cells and osteoblasts: Evidence for HDAC2 involvement. Stem Cells 2014;32:279–289.

15 Schroeder TM, Kahler RA, Li X et al. Histone deacetylase 3 interacts with runx2 to repress the osteocalcin promoter and regulate osteoblast differentiation. J Biol Chem 2004;279:41998–42007.

16 Vega RB, Matsuda K, Oh J et al. Histone deacetylase 4 controls chondrocyte hypertrophy during skeletogenesis. Cell 2004; 119:555–566.

17 Li H, Xie H, Liu W et al. A novel microRNA targeting HDAC5 regulates osteoblast differentiation in mice and contributes to primary osteoporosis in humans. J Clin Invest 2009;119:3666–3677.

18 Westendorf JJ, Zaidi SK, Cascino JE et al. Runx2 (Cbfa1, AML-3) interacts with histone deacetylase 6 and represses the p21 (CIP1/WAF1) promoter. Mol Cell Biol 2002;22: 7982–7992.

19 Jensen ED, Gopalakrishnan R, Westendorf JJ. Bone morphogenic protein 2 activates protein kinase D to regulate histone deacetylase 7 localization and repression of Runx2. J Biol Chem 2009;284:2225–2234.

20 Haberland M, Mokalled MH, Montgomery RL et al. Epigenetic control of skull morphogenesis by histone deacetylase 8. Genes Dev 2009;23:1625–1630.

21 Fu Y, Zhang P, Ge J et al. Histone deacetylase 8 suppresses osteogenic differentiation of bone marrow stromal cells by inhibiting histone H3K9 acetylation and RUNX2 activity. Int J Biochem Cell Biol 2014; 54:68–77.

22 Marie PJ, de Pollak C, Chanson P et al. Increased proliferation of osteoblastic cells expressing the activating Gs alpha mutation in monostotic and polyostotic fibrous dysplasia. Am J Pathol 1997;150:1059–1069.

23 Kloster MM, Naderi EH, Haaland I et al. cAMP signalling inhibits p53 acetylation and apoptosis via HDAC and SIRT deacetylases. Int J Oncol 2013;42:1815–1821.

24 Oehme I, Deubzer HE, Wegener D et al. Histone deacetylase 8 in neuroblastoma tumorigenesis. Clin Cancer Res 2009;15: 91–99.

25 Wu J, Du C, Lv Z et al. The up-regulation of histone deacetylase 8 promotes proliferation and inhibits apoptosis in hepatocellular carcinoma. Dig Dis Sci 2013; 58:3545–3553.

26 Shi RR, Li XF, Zhang R et al. *GNAS* mutational analysis in differentiating fibrous dysplasia and ossifying fibroma of the jaw. Mod Pathol 2013;26:1023–1031.

27 Ge J, Guo S, Fu Y et al. Dental follicle cells participate in tooth eruption via the RUNX2-MiR-31-SATB2 loop. J Dent Res 2015; 94:936–944.

28 Xu R, Fu Z, Liu X et al. Transplantation of osteoporotic bone marrow stromal cells rejuvenated by the overexpression of SATB2 prevents alveolar bone loss in ovariectomized rats. Exp Gerontol 2016;84:71–79.

29 JFt B, Brownlow RC, Leith JP et al. Bupivacaine inhibits cyclic-3′,5′-adenosine monophosphate production. A possible contributing factor to cardiovascular toxicity. Anesthesiology 1993;79:88–95.

30 Riminucci M, Saggio I, Robey PG et al. Fibrous dysplasia as a stem cell disease. J Bone Miner Res 2006;21(Suppl 2):P125–P131.

31 Schwindinger WF, Francomano CA, Levine MA. Identification of a mutation in the gene encoding the alpha subunit of the stimulatory G protein of adenylyl cyclase in McCune-Albright syndrome. Proc Natl Acad Sci USA 1992;89:5152–5156.

32 Parekh SG, Donthineni-Rao R, Ricchetti E et al. Fibrous dysplasia. J Am Acad Orthop Surg 2004;12:305–313.

33 Walia MK, Ho PM, Taylor S et al. Activation of PTHrP-cAMP-CREB1 signaling following p53 loss is essential for osteosarcoma initiation and maintenance. Elife 2016;5: e13446.

34 Ramaswamy G, Kim H, Zhang D et al. Gsalpha controls cortical bone quality by regulating osteoclast differentiation via cAMP/PKA and beta-catenin pathways. Sci Rep 2017;7:45140.

35 Silve C. Genes in the cAMP pathway causing skeletal dysplasia with or without hormonal resistance. Biol Aujourdhui 2016; 210:167–170.

36 Rosenberg D, Groussin L, Jullian E et al. Role of the PKA-regulated transcription factor CREB in development and tumorigenesis of endocrine tissues. Ann N Y Acad Sci 2002;968:65–74.

37 Wang R, Li G, Liu C et al. Three-dimensional printing of reduction template in the contouring of craniofacial fibrous dysplasia. J Craniofac Surg 2016;27:1792–1794.

38 Gao J, Siddoway B, Huang Q et al. Inactivation of CREB mediated gene transcription by HDAC8 bound protein phosphatase. Biochem Biophys Res Commun 2009;379:1–5.

39 Boyce AM, Chong WH, Yao J et al. Denosumab treatment for fibrous dysplasia. J Bone Miner Res 2012;27:1462–1470.

40 Chapurlat RD. Medical therapy in adults with fibrous dysplasia of bone. J Bone Miner Res 2006;21(suppl 2):P114–P119.

41 Rettig I, Koeneke E, Trippel F et al. Selective inhibition of HDAC8 decreases neuroblastoma growth in vitro and in vivo and enhances retinoic acid-mediated differentiation. Cell Death Dis 2015;6:e1657.

42 Debeb BG, Lacerda L, Xu W et al. Histone deacetylase inhibitors stimulate dedifferentiation of human breast cancer cells through WNT/beta-catenin signaling. Stem Cells 2012;30:2366–2377.

43 Huang HY, Liu DD, Chang HF et al. Histone deacetylase inhibition mediates urocortin-induced antiproliferation and neuronal differentiation in neural stem cells. Stem Cells 2012;30:2760–2773.

44 Huynh NC, Everts V, Nifuji A et al. Histone deacetylase inhibition enhances in-vivo bone regeneration induced by human periodontal ligament cells. Bone 2017;95:76–84.

45 Lopez G, Bill KL, Bid HK et al. HDAC8, a potential therapeutic target for the treatment of malignant peripheral nerve sheath tumors (MPNST). PLoS One 2015;10:e0133302.

46 Balasubramanian S, Ramos J, Luo W et al. A novel histone deacetylase 8 (HDAC8)-specific inhibitor PCI-34051 induces apoptosis in T-cell lymphomas. Leukemia 2008;22: 1026–1034.

47 Saggio I, Remoli C, Spica E et al. Constitutive expression of Gsalpha(R201C) in mice produces a heritable, direct replica of human fibrous dysplasia bone pathology and demonstrates its natural history. J Bone Miner Res 2014;29:2357–2368.

48 Saloustros E, Liu S, Mertz EL et al. Celecoxib treatment of fibrous dysplasia (FD) in a human FD cell line and FD-like lesions in mice with protein kinase A (PKA) defects. Mol Cell Endocrinol 2017;439:165–174.

49 Zhao X, Deng P, Iglesias-Bartolome R et al. Expression of an active Galphas mutant in skeletal stem cells is sufficient and necessary for fibrous dysplasia initiation and maintenance. Proc Natl Acad Sci USA 2018;115: E428–E437.

50 Kamalaldin N, Jaafar M, Zubairi SI et al. Physico-mechanical properties of HA/TCP pellets and their three-dimensional biological evaluation in vitro. Adv Exp Med Biol 2018: pp 1–15.

51 Castilho M, Moseke C, Ewald A et al. Direct 3D powder printing of biphasic calcium phosphate scaffolds for substitution of complex bone defects. Biofabrication 2014;6: 015006.

52 Detsch R, Mayr H, Ziegler G. Formation of osteoclast-like cells on HA and TCP ceramics. Acta Biomater 2008;4:139–148.

See www.StemCellsTM.com for supporting information available online.